machines

MDPI

Article

Horizontal and Vertical Coordinated Control of Three-Axis Heavy Vehicles

Lanchun Zhang [1,*], Fei Huang [2], Hao Cui [2], Yaqi Wang [2] and Lin Yang [1]

[1] School of Automotive & Traffic Engineering, Jiangsu University of Technology, Changzhou 213001, China; yanglin928@jsut.edu.cn
[2] School of Mechanical Engineering, Jiangsu University of Technology, Changzhou 213001, China; 2024655206@smail.jsut.edu.cn (F.H.); 2023655026@smail.jsut.edu.cn (H.C.); 2023655036@smail.jsut.edu.cn (Y.W.)
* Correspondence: zlc@jsut.edu.cn

Abstract: In order to coordinate the transverse motion control and longitudinal motion control in the tracking control process and ensure the yaw stability and roll stability in the tracking process, a transverse and longitudinal coordinated control method of three-axis heavy vehicles is designed based on model predictive control. The lateral motion controller is designed based on the phase plane method. The upper controller calculates the front wheel angle and additional yaw moment, which ensures the yaw stability while tracking the vehicle. The lower controller calculates the driving force and braking force of the three-axis heavy vehicle. The velocity planning method is designed with the coupling point of longitudinal velocity to coordinate the lateral and longitudinal motion controllers and prevent vehicle rollover. By building the vehicle model in Trucksim (2016.1) and establishing the horizontal and vertical coordination control in Matlab (R2016b), the designed horizontal and vertical coordination control method is simulated and verified. The simulation results show that the designed method can accurately track the reference trajectory while ensuring the yaw stability and roll stability of the three-axis heavy vehicle.

Keywords: three-axis dump truck; tracking control; horizontal and vertical coordinated control strategy; real-time speed profile planning; model predictive control

check for updates

Academic Editor: Francesco Castellani

Received: 30 December 2024
Revised: 2 February 2025
Accepted: 5 February 2025
Published: 7 February 2025

Citation: Zhang, L.; Huang, F.; Cui, H.; Wang, Y.; Yang, L. Horizontal and Vertical Coordinated Control of Three-Axis Heavy Vehicles. *Machines* **2025**, *13*, 123. https://doi.org/10.3390/machines13020123

Copyright: © 2025 by the authors. Licensee MDPI, Basel, Switzerland. This article is an open access article distributed under the terms and conditions of the Creative Commons Attribution (CC BY) license (https://creativecommons.org/licenses/by/4.0/).

1. Introduction

With the rapid establishment of highway networks, the road transportation industry, especially the logistics and transportation system centered on heavy vehicles (including tanker trucks, heavy semi-trailers, etc.), has witnessed a booming development. However, compared to passenger cars, heavy vehicles are characterized by rear amplification due to their high center of gravity position, large weight and volume, significant body length, and structural complexity, such as the complex coupling relationship between the tractor and the trailer truck in heavy semi-trailers, which makes these vehicles face more severe safety challenges during driving.

Heavy vehicles have obvious shortcomings in terms of maneuvering flexibility and stability, which directly leads to the fact that they are prone to serious accidents, such as rollover; pendulum vibration; and folding under complex working conditions such as high-speed driving, emergency braking, and sharp turning, and the resulting damages if an accident occurs are greater than those of a regular vehicle; according to data released by the National Highway Traffic Safety Administration, in 2017, rollovers produced 17.1% of all fatal accidents in the U.S., with 591 (12.7%) of those being large truck rollover accidents,

and when the vehicle loses its traverse stability, dangerous situations such as sideslip and rollover are prone to occur, resulting in the vehicle deviating from the expected trajectory. Therefore, it is necessary to improve the traverse stability and anti-rollover performance of heavy vehicles in the tracking control process to ensure that the vehicle will not go out of control.

In this context, the coordinated horizontal and vertical control of heavy vehicles is particularly important. This coordinated control mechanism aims to realize the integrated control of the horizontal and vertical motions of the vehicle by precisely regulating the suspension system, steering system, driving/braking system, and other key components of the vehicle, thus significantly improving the driving stability of the vehicle. Specifically, the horizontal and vertical coordinated control can monitor key parameters such as the vehicle's sway angular velocity, lateral acceleration, lateral inclination angle, lateral inclination moment, etc. in real time and realize the real-time correction of the vehicle's attitude by adjusting the suspension system's stiffness and damping and the steering system's responsiveness, as well as the distribution of the driving/braking force, effectively suppressing the sway and lateral inclination movements and improving the vehicle's sway stability and anti-rollover performance.

In the traditional heavy vehicle stability control, the mainstream methods mainly include a rollover warning system, active suspension or semi-active suspension, and other technologies to improve the heavy vehicle lateral tilt and sway stability and reduce the accident rate.

Drivers often have no time to react when heavy vehicles roll over, so early warning of vehicle rollover is undoubtedly a good way to avoid risks. Foreign scholars have conducted extensive research on vehicle rollover warning systems in this field [1–4].

In 2014, Yi Hua Chen established a car rollover prediction model and designed a car rollover warning system by calculating the TTR vehicle rollover prediction algorithm. The experimental results showed that the TTR rollover prediction method can provide guidance for drivers [5].

In 2022, Pei Pei Chao et al. proposed an improved rolling time method based on multilayer neural networks, focusing on household cars. They established and analyzed a force model of a car rollover, simplified the algorithm structure of the rolling time using multilayer neural networks, and quickly calculated the operating state parameters with changing step sizes in real time. The experiment studied the influence of hyperparameters on the prediction results of neural networks, and compared to the traditional prediction methods, the prediction efficiency was higher [6]. Junjian Hou proposed a new rollover indicator based on the comprehensive roll angle of tractors and trailers, which uses the Unscented Kalman Filter (UKF) algorithm to estimate the roll angle of tracks and trailers. A two-stage rollover warning method triggered by video and audio is used to reduce false alarms, and the effectiveness of the proposed rollover warning method is verified through joint simulation [7]. Xinwei Yang improved the dynamic rollover index for detecting real-time rollover events under trip and non-trip conditions and designed a parameter estimation algorithm based on the Normalized Least Mean Square (NLMS) for unmeasurable time-varying parameters [8]. Ruiyang Wang selected the lateral load transfer rate (LTR) of the vehicle as the warning algorithm for vehicle rollover and used the vehicle's rollover attitude as a reference, combined with the fuzzy PID control algorithm, to achieve vehicle deceleration balance control. Finally, a vehicle dynamics model was established to verify the effectiveness of the control strategy under extreme working conditions [9].

The active suspension system [10,11] provides active torque through hydraulic actuators to control the vehicle's lateral motion during turns, thereby stabilizing the vehicle. Li Haiqing et al. used the predictive load transfer ratio (PLTR) as a rollover indicator to design

an active suspension control system for anti-rollover based on rollover prediction and fuzzy proportional integral derivative (PID). The fuzzy PID controller is only activated when the likelihood of rollover measured by the PLTR is high. The research results indicate that the PLTR index can provide an indicator for early measurement of the rollover tendency, and the fuzzy PID anti-rollover control algorithm of the PLTR index has better rollover stability compared to traditional load transfer ratio indicators [12]. Liang et al. proposed a decentralized collaborative control framework that integrates active front steering and active suspension systems by applying a multi-constraint distributed model predictive control method, aiming to improve vehicle lateral stability, ride comfort, and roll safety during path tracking [13]. However, most of the above methods only explore the vehicle's anti-rollover performance and do not take into account the vehicle's lateral stability.

Many scholars have studied how to improve the lateral stability and anti-rollover performance of vehicles. Ahmadian N et al. proposed a comprehensive adaptive coordination method that combines active front wheel steering (AFS) and direct yaw torque control (DYC) [14]. This method can effectively reduce the angle of vehicle sideslip and lateral acceleration. Peng H et al. proposed a robust model predictive control with a limited time range to coordinate the path tracking controller and the direct yaw moment controller [15]. A linear variable parameter discrete model was constructed considering the time-varying and uncertain characteristics of tire corner stiffness and vehicle speed. Based on the linear matrix inequality method, a new robust MPC theory was proposed for the real-time updating of four convex hull vertices to solve optimization problems. The experimental results demonstrate that this method enhances the robustness of the control system. Qian X et al. developed a comprehensive control system based on fuzzy differential braking for the lateral and roll stability control of non-pneumatic mechanical elastic wheel off-road vehicles [16]. The upper level comprehensive control algorithm adopts a fuzzy proportional integral differential to coordinate the yaw and roll control simultaneously. The lower control distributor generates an additional lateral moment of the vehicle through differential braking. This method can improve the vehicle's lateral stability and roll stability, preventing rollover. However, the methods used in the above studies were all designed for two-axle vehicles.

Bailin Fan designed a radial basis function neural network sliding mode controller for intelligent fire trucks, which improved the accuracy of vehicle path tracking [17]. Feng Zhao adopted a hierarchical control framework and proposed an adaptive predictive time linear quadratic regulator (APT LQR) path following algorithm in the upper controller to obtain the required front wheel steering angle [18]. The lateral stability of DDAUV is determined based on the phase plane, and in the improved sliding mode control (SMC), the sliding surface is further dynamically adjusted to obtain the required additional yaw moment for coordinating path following and lateral stability. Then, in the lower controller, a comprehensive cost function was established to reasonably allocate the driving torque of the four hub motors, thereby generating the required additional yaw torque. This method can effectively coordinate path following and lateral stability. Aman Parkash proposed a control scheme to improve the lane keeping activity performance of an autonomous vehicle within the guaranteed deviation range, which improved the controllability of vehicles [19]. Qin Z et al. proposed a lateral and longitudinal dynamics control framework for an autonomous vehicle considering multi-parameter joint estimation. Through the collaborative simulation of PreScan and CarSim, the proposed estimation and control framework was preliminarily verified. Through experiments on the autonomous vehicle platform—hybrid Lincoln MKZ—the estimated control framework has excellent performance and improved tracking accuracy and lateral stability [20]. Amauri Da Silva Junior used a sliding mode control to improve the longitudinal stability of a vehicle [21], while Lin Zhang used hierarchical

control to enhance the stability and anti-interference performance of an entire vehicle [22]. The above study only considered single lateral or longitudinal control and did not take into account longitudinal and transverse coordinated control.

Sathyamangalam et al. [23] studied the mechanism of car rollover [24–26] and used a reverse steering mechanism to prevent vehicle rollover. Speed planning calculated the target speed curve to ensure that the vehicle meets the requirements of handling stability and smoothness [27]. Luo Y et al. proposed a new optimal speed consultation strategy for continuous intersections, which helps to reduce fuel consumption and passage time [28]. Easa S et al. discussed the problem of reasonable allocation of overtaking speed when overtaking on a dual lane highway and used the finite element method to optimize the speed distribution of passing vehicles during the overtaking process [29]. Zhang S et al. proposed a speed planning method based on piecewise quadratic polynomial curves [30]. This method divides the quadratic polynomial curve under different velocity constraints and adjusts the rate of acceleration change of the local velocity curve. The above speed planning methods did not take into account the impact of vehicle speed on vehicle rollover.

Three-axis heavy-duty vehicles have a large load capacity, good stability performance, and fast driving speed, and most of the current kinetic modeling by scholars at home and abroad is based on four-wheeled vehicles or two-axis vehicles, but relatively few studies have been conducted on three-axis vehicles, and most of the current research on three-axis heavy-duty vehicles only consider a single transverse control or longitudinal control, but the cross-swing stability and anti-rollover performance of heavy-duty vehicles are the focus of attention required for the operation of the vehicle, and there is still a lot of research space for coordinated longitudinal and transverse control of heavy-duty vehicles. In addition, the effect of speed on the rollover of a vehicle cannot be ignored. Therefore, this paper proposes a coordinated longitudinal and transverse control method for a three-axis heavy-duty vehicle to plan a velocity profile considering the rollover stability of the heavy-duty vehicle and to coordinate the transverse motion control and longitudinal motion control during tracking so as to improve the smoothness of the three-axis heavy-duty vehicle.

In order to coordinate lateral motion control and longitudinal motion control during the tracking control process and ensure the lateral stability and roll stability during the tracking process, this paper takes a three-axis heavy-duty vehicle as the research object. Based on model predictive control, real-time speed planning and lateral and longitudinal coordination control methods are studied. Through the coordination of steering, braking, and other modules, the three-axis heavy-duty vehicle can accurately track the desired trajectory while ensuring lateral stability and roll stability during the tracking process.

The remaining parts of this article are organized as follows. Section 2 analyzes the dynamic model of three-axis heavy-duty vehicles, including establishing vehicle dynamics equations and building tire models. Section 3 designs a lateral motion control and stability controller that combines active steering and differential braking based on the phase plane method. The lateral motion controller and longitudinal motion controller are introduced in detail. In order to improve the roll stability of three-axis heavy-duty vehicles during tracking control, a real-time speed planning method is proposed. Section 4 establishes a joint simulation model of Trucksim and Simulink and conducts simulation experiments on three-axle heavy-duty vehicles under constant speed control conditions and coordinated longitudinal and transverse control conditions, respectively. Section 5 summarizes the entire text.

2. Three-Axis Heavy Vehicle Dynamics Model

2.1. Vehicle Dynamics Equations

The vehicle dynamics model developed in this paper is used for the transverse–longitudinal coordinated control of the vehicle. In order to simplify the control, the following simplifications and assumptions are made.

(1) The vehicle is driven on a flat road, and the effect of road slope on the vehicle motion is neglected.

(2) We neglected the effect of air resistance on the vehicle.

(3) Only the steering angle of the front wheels changes during vehicle steering, and the steering angles of the left and right front wheels are the same.

(4) Assume that the vehicle front and rear axle lateral tilt center is equal and distributed along the longitudinal symmetry of the car.

(5) Ignore the role of wheel return torque and positioning parameters.

A four-degree-of-freedom dynamics model of a three-axis heavy vehicle is developed for the real-time velocity planning method and the design of a lateral motion controller. The four degrees of freedom are the longitudinal, lateral, transverse, and lateral motion of the vehicle, as shown in Figure 1.

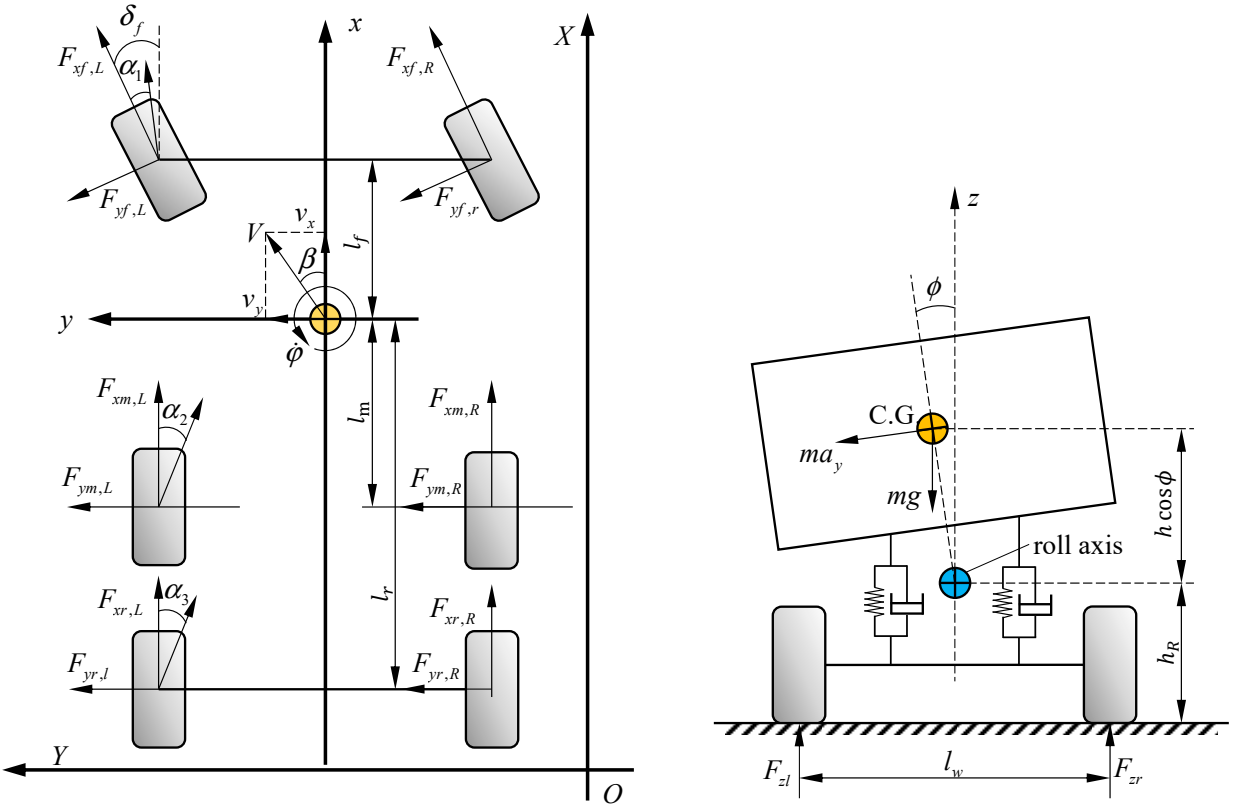


Figure 1. Four-degrees-of-freedom model of a three-axis heavy vehicle.

The four-degree-of-freedom dynamics equation for a three-axle heavy vehicle is

$$\begin{aligned} &m\dot{v}_x = mv_y(\dot{\varphi} + \dot{\beta}) + F_{xf}\cos\delta_f \\ &-F_{yf}\sin\delta_f + F_{xm} + F_{xr} \end{aligned} \tag{1}$$

$$\begin{aligned} &m\dot{v}_y = -mv_x(\dot{\varphi} + \dot{\beta}) + mh\ddot{\phi} + F_{xf}\sin\delta_f \\ &+F_{yf}\cos\delta_f + F_{ym} + F_{yr} \end{aligned} \tag{2}$$

$$\dot{\beta} = \frac{\sin\beta}{mv}F_x + \frac{\cos\beta}{mv}F_y - \dot{\varphi} \tag{3}$$

$$I_z\ddot{\varphi} = l_f(F_{xf}\sin\delta_f + F_{yf}\cos\delta_f) - F_{ym}l_m - F_{yr}l_r + M \tag{4}$$

$$\begin{aligned}(I_x + mh^2)\ddot{\phi} &= ma_y h\cos\phi + mgh\sin\phi \\ &-0.5K_\phi {l_w}^2\sin\phi - 0.5C_\phi {l_w}^2\dot{\phi}\cos\phi\end{aligned} \tag{5}$$

Among

$$\begin{aligned}F_{xf} &= F_{xf,L} + F_{xf,R} \\ F_{xm} &= F_{xm,L} + F_{xm,R} \\ F_{xr} &= F_{xr,L} + F_{xr,R}\end{aligned} \tag{6}$$

$$\begin{aligned}F_{yf} &= F_{yf,L} + F_{yf,R} \\ F_{ym} &= F_{ym,L} + F_{ym,R} \\ F_{yr} &= F_{yr,L} + F_{yr,R}\end{aligned} \tag{7}$$

where m is the spring-loaded mass; v_x and v_y are the velocities of the center of mass in the x and y directions of the vehicle coordinate system, respectively; φ is the vehicle transverse sway angle; φ is the vehicle roll angle; F_{xf*}, F_{xm*}, and F_{xr*} are the longitudinal forces on the front, middle, and rear wheels of the vehicle, respectively; $F_{\mathrm{yf}*}$, F_{ym*}, and F_{yr*} are the lateral forces on the front, middle, and rear wheels of the vehicle, respectively; δ_f is the front wheel turning angle; K_φ is the suspension equivalent lateral sway stiffness; C_φ is the suspension equivalent lateral sway damping; h is the lateral sway arm length; I_x and I_z are the vehicle rotational inertia around the x- and z-axes, respectively; l_w is the body width; and M is the additional transverse sway dip moment; * = {L, R}.

The projection of the vehicle longitudinal and lateral velocities in the x and y directions of the world coordinate system yields is as follows:

$$\dot{X} = v_x\cos\varphi - v_y\sin\varphi \tag{8}$$

$$\dot{Y} = v_x\sin\varphi + v_y\cos\varphi \tag{9}$$

2.2. Tire Model

The tire steady-state model describes the longitudinal slip and lateral deflection characteristics of the tire steady-state motion process. According to the magic formula [31], the formula for the longitudinal force of the tire is as follows:

$$F_x = (D\sin(\mathrm{C}\arctan(BX_1 - E(BX_1 - \arctan(BX_1))))) + S_v \tag{10}$$

Among them,

$$\begin{cases} C = B_0 \\ D = B_1F_z^2 + B_2F_z \\ BCD = \left(B_3F_z^2 + B_4F_z\right)\times e^{-B_5F_z} \\ E = B_6F_z^2 + B_7F_z + B_8 \\ X_1 = s + S_h \\ S_h = B_9F_z + B_{10} \\ S_v = 0 \end{cases} \tag{11}$$

The formula for calculating the lateral force of the tire is

$$F_y = (D\sin(\mathrm{C}\arctan(BX_1 - E(BX_1 - \arctan(BX_1))))) + S_v \tag{12}$$

Among others,

$$\begin{cases} C = A_0 \\ D = A_1 F_z^2 + A_2 F_z \\ BCD = A_3 \sin(2\arctan\frac{F_z}{A_4}) \times (1 - A_5|\gamma|) \\ E = A_6 F_z + A_7 \\ X_1 = \alpha + S_h \\ S_h = A_9 F_z + A_{10} + A_8 \gamma \\ S_v = A_{11} F_z \gamma + A_{12} F_z + A_{13} \end{cases} \tag{13}$$

A_0~A_{13} and B_0~B_{10} can be obtained experimentally and are shown in Table 1.

Table 1. Magic formula parameter-taking values.

Parameter	Value	Parameter	Value
A_0	1.65	A_7	0.77394
A_1	−34	A_8	0.002289
A_2	1250	A_9	0.013442
A_3	3036	A_{10}	0.0037
A_4	12.8	A_{11}	19.1656
A_5	0.00501	A_{12}	1.21356
A_6	−0.02103	A_{13}	6.26206
B_0	2.37272	B_7	−0.0615
B_1	−9.46	B_8	1.2
B_2	1490	B_9	0.0299
B_3	130	B_{10}	−0.176
B_4	276		
B_5	0.0886		
B_6	0.00402		

The formula for calculating the slip rate in the magic formula tire model is

$$s_{f*} = \frac{\omega_t r - v_{f*}}{v_{f*}} \times 100\% \tag{14}$$

where * = {m, r}.

The longitudinal acceleration, lateral acceleration, and lateral motion of the spring-loaded mass during the steering movement of the vehicle have an effect on the vertical load of each wheel. The vertical loads on each wheel of a three-axle heavy vehicle are

$$\begin{cases} F_{z,fL} = (\frac{mg}{2} - \frac{ma_y h_c}{l_w})\frac{d}{L} - \frac{ma_x h_c}{2L} - (\frac{1}{2}K_\phi l_w \sin\phi + \frac{1}{2}C_\phi l_w \dot{\phi}\cos\phi)\frac{d}{L} \\ F_{z,fR} = (\frac{mg}{2} + \frac{ma_y h_c}{l_w})\frac{d}{L} - \frac{ma_x h_c}{2L} + (\frac{1}{2}K_\phi l_w \sin\phi + \frac{1}{2}C_\phi l_w \dot{\phi}\cos\phi)\frac{d}{L} \\ F_{z,mL} = (\frac{mg}{2} - \frac{ma_y h_c}{l_w})\frac{l_f}{2L} + \frac{ma_x h_c}{4L} - (\frac{1}{2}K_\phi l_w \sin\phi + \frac{1}{2}C_\phi l_w \dot{\phi}\cos\phi)\frac{l_f}{2L} \\ F_{z,mR} = (\frac{mg}{2} + \frac{ma_y h_c}{l_w})\frac{l_f}{2L} + \frac{ma_x h_c}{4L} + (\frac{1}{2}K_\phi l_w \sin\phi + \frac{1}{2}C_\phi l_w \dot{\phi}\cos\phi)\frac{l_f}{2L} \\ F_{z,rL} = (\frac{mg}{2} - \frac{ma_y h_c}{l_w})\frac{l_f}{2L} + \frac{ma_x h_c}{4L} - (\frac{1}{2}K_\phi l_w \sin\phi + \frac{1}{2}C_\phi l_w \dot{\phi}\cos\phi)\frac{l_f}{2L} \\ F_{z,rR} = (\frac{mg}{2} + \frac{ma_y h_c}{l_w})\frac{l_f}{2L} + \frac{ma_x h_c}{4L} + (\frac{1}{2}K_\phi l_w \sin\phi + \frac{1}{2}C_\phi l_w \dot{\phi}\cos\phi)\frac{l_f}{2L} \end{cases} \tag{15}$$

Among them, $d = (l_m + l_r)/2$, and $L = l_f + d$.

The longitudinal velocity of each wheel center in the wheel coordinate system is as follows:

$$\begin{cases} v_{f,L} = (v_x - \frac{l_w}{2}\dot{\varphi})\cos\delta_f + (v_y + l_f\dot{\varphi})\sin\delta_f \\ v_{f,R} = (v_x + \frac{l_w}{2}\dot{\varphi})\cos\delta_f + (v_y + l_f\dot{\varphi})\sin\delta_f \\ v_{m,L} = v_{r,L} = v_x - \frac{l_w}{2}\dot{\varphi} \\ v_{m,R} = v_{r,R=}v_x + \frac{l_w}{2}\dot{\varphi} \end{cases} \tag{16}$$

The tire side deflection angle can be approximated as

$$\alpha_f = \frac{v_y + l_f\dot{\varphi}}{v_x} - \delta_f \tag{17}$$

$$\alpha_m = \frac{v_y - l_m\dot{\varphi}}{v_x} \tag{18}$$

$$\alpha_r = \frac{v_y - l_r\dot{\varphi}}{v_x} \tag{19}$$

3. Horizontal and Vertical Coordination Control

The actual driving process of the vehicle speed is constantly changing, with starting, stopping, and other situations. Under the dangerous working conditions such as a large road curvature and low road surface adhesion coefficient, the vehicle should reduce the speed to pass the dangerous section at a safer speed. In addition, considering the strong coupling characteristics between the transverse and longitudinal dynamics of the vehicle, the speed planning method is designed with the longitudinal speed as the coupling point to coordinate the transverse and longitudinal motion controllers, so that the three-axis heavy-duty vehicle can track the reference trajectory under variable speed conditions while ensuring stability during driving.

A lateral motion control and stability controller combining active steering and differential braking is designed based on the phase plane method, which performs lateral stability control of the three-axle heavy-duty vehicle while tracking the reference path and determines the stability boundary of the vehicle based on the phase plane method. When the state of the three-axle heavy vehicle does not exceed the stability boundary, the braking torque of each wheel is uniformly distributed. When the three-axle heavy vehicle exceeds the stability boundary, the controller generates additional transverse sway moments while tracking the reference path to ensure the lateral stability of the three-axle heavy vehicle. The additional transverse moment is achieved by differential braking, and the braking force is distributed, taking into account constraints such as tire force utilization. Secondly, a speed planning method considering the lateral stability of the three-axle heavy vehicle is designed, which calculates the upper limit of the longitudinal speed based on the lateral load transfer rate of the vehicle at the current moment and the road curvature at the pre-sighting point and plans a speed curve from the starting point to the end point and makes it meet the requirements of the vehicle lateral stability and speed and acceleration limits.

The horizontal and vertical coordination control framework is shown in Figure 2.

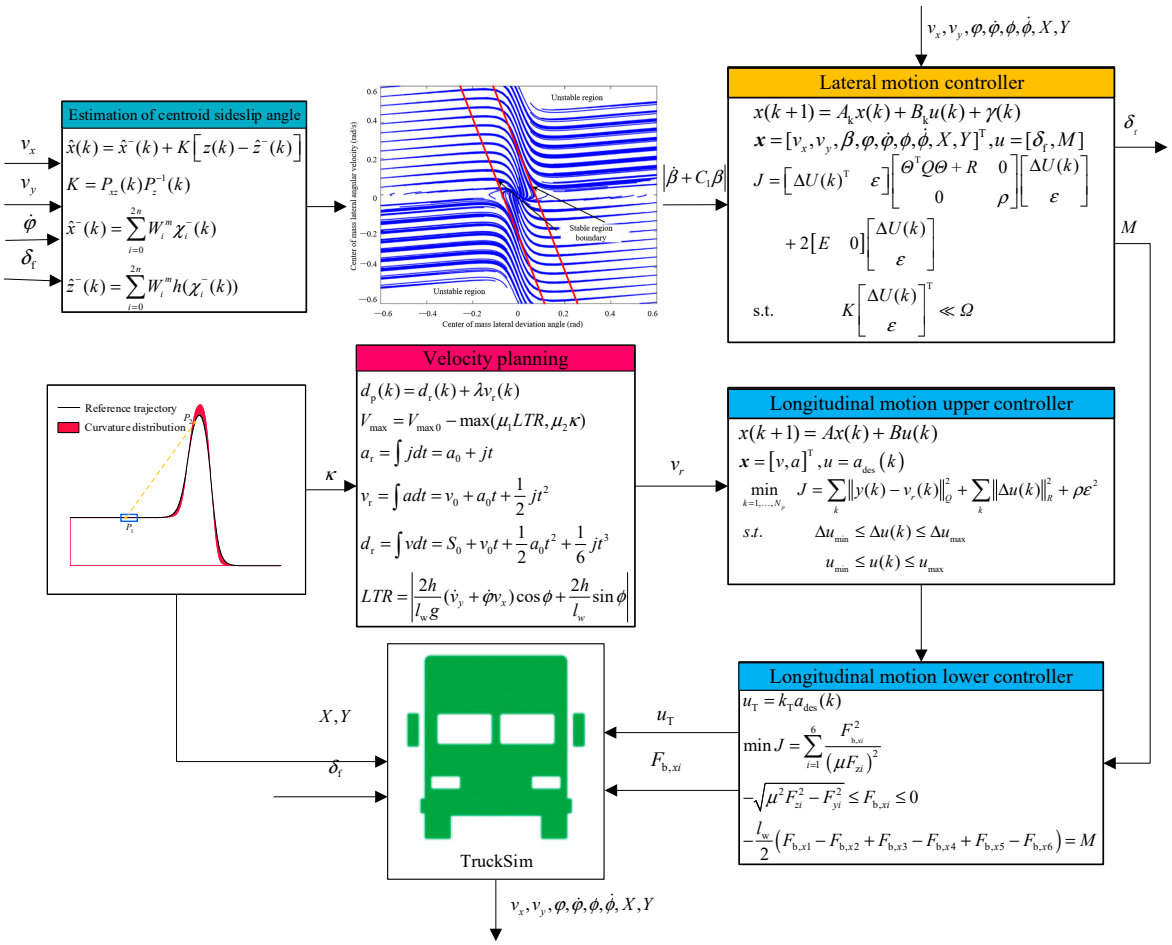


Figure 2. Framework of variable speed transverse–longitudinal coordination control.

3.1. Phase Plane

Before lateral stability control can be performed on a three-axle heavy vehicle, the lateral stability of the vehicle needs to be judged. The $\beta - \dot{\beta}$ phase plane is divided into stable and unstable regions, which reflect the influence of the initial state of the vehicle on the subsequent vehicle trajectory, as shown in Figure 3.

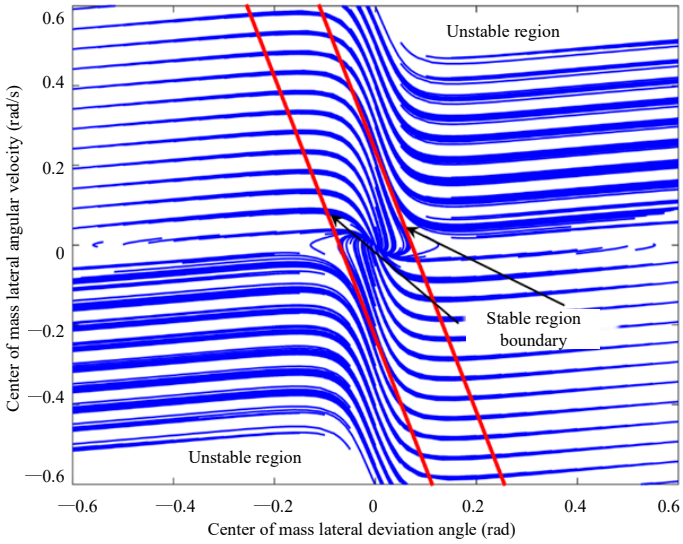


Figure 3. The$\beta - \dot{\beta}$ phase plane.

The vehicle starts running from any point in the stability zone, and the ride is always stable. If the vehicle is in an unstable region, the vehicle can only be brought back into the stability region by an additional lateral stability control algorithm.

The factors affecting the stability boundary of the $\beta - \dot{\beta}$ phase plane mainly include the road surface adhesion coefficient, vehicle speed, and front wheel turning angle, but the effects of vehicle speed and front wheel turning angle are negligible in practical applications. The phase plane based stability domain boundary delineation mainly includes a two-line method, bifold method, five eigenvalue rhombus method, and limit ring method. Compared to other methods, the two-line method has a simple structure and uses fewer parameters, so the two-line method is used in this paper to determine the boundary of the stability domain of the phase plane drawn based on the eccentric angle of the mass side and the eccentric velocity of the mass side.

When the road surface adhesion coefficient is constant, the condition of the bilinear method regarding the lateral stability of the vehicle can be expressed as

$$\left|\dot{\beta} + C_1\beta\right| < C_2 \tag{20}$$

where C_1 and C_2 are the stability boundary coefficients, representing the intercept and slope of the stability boundary in the phase plane, respectively.

3.2. Transverse Motion Controller Design

From Equations (1)–(7), it is obtained that

$$\begin{cases} \dot{\boldsymbol{x}} = f(\boldsymbol{x}, \boldsymbol{u}) \\ \boldsymbol{y} = C\boldsymbol{x} \end{cases} \tag{21}$$

The system state quantity is $\boldsymbol{x} = [v_x, v_y, \beta, \varphi, \dot{\varphi}, \phi, \dot{\phi}, X, Y]^{\mathrm{T}}$, the system control quantity is $\boldsymbol{u}$ = [δ_{f}, M], and the system output is $\boldsymbol{y}$ = [β, φ, Y].

Apply Taylor expansion to Equation (16) at the operating point ($x_0(t)$, $u_0(t-1)$) to linearize the nonlinear vehicle dynamics model as follows:

$$\dot{\boldsymbol{x}}(t) = f(\boldsymbol{x}_0(t), \boldsymbol{u}_0(t-1)) + \boldsymbol{A}_t(\boldsymbol{x}(t) - \boldsymbol{x}_0(t)) + \boldsymbol{B}_t(\boldsymbol{u}(t) - \boldsymbol{u}_0(t-1)) \tag{22}$$

At the sampling moment t, the discrete linear time-varying state equation and the output equation are obtained by discretizing Equation (22) through the forward difference method as follows:

$$\begin{aligned} x(k+1) &= A_k x(k) + B_k u(k) + \gamma(k) \\ y(k) &= C_k x(k) \end{aligned} \tag{23}$$

where

$$A_k = A_t T + I \tag{24}$$

$$B_k = B_t T \tag{25}$$

$$A_t = \left.\frac{\partial f}{\partial x}\right|_{(x_0(t), u_0(t-1))} \tag{26}$$

$$B_t = \left.\frac{\partial f}{\partial x}\right|_{(x_0(t), u_0(t-1))} \tag{27}$$

$$C_k = \begin{bmatrix} 0 & \frac{1}{v_c} & 0 & 0 & 0 & 0 & 0 & 0 \\ 0 & 0 & 0 & 0 & K_\phi & C_\phi & 0 & 0 \\ 0 & 0 & 1 & 0 & 0 & 0 & 0 & 0 \\ 0 & 0 & 0 & 0 & 0 & 0 & 0 & 1 \end{bmatrix} \tag{28}$$

$$\gamma(k) = f(x_0(k), u_0(k-1)) - A_t x_0(k) - B_t u_0(k-1) \tag{29}$$

In addition to calculating the magnitude of the control quantity, the control increment $\Delta \boldsymbol{u}(\mathrm{k}) = \boldsymbol{u}(k) - \boldsymbol{u}(k-1)$ is introduced in order to be able to control the rate of change of the control quantity as well. Equation (23) can be transformed as follows:

$$\begin{cases} \xi(k+1) = \widetilde{A}_k \xi(k) + \widetilde{B}_k \Delta u(k) + \widetilde{\gamma}(k) \\ \eta(k) = C_k \xi(k) \end{cases} \tag{30}$$

where

$$\begin{cases} \xi(k) = \begin{bmatrix} x(k) & u(k-1) \end{bmatrix}^T \\ \widetilde{A}_k = \begin{bmatrix} A_k & B_k \\ 0 & I \end{bmatrix} \\ \widetilde{B}_k = \begin{bmatrix} B_k & I \end{bmatrix}^T \\ \widetilde{C}_k = \begin{bmatrix} C_k & 0 \end{bmatrix}^T \\ \widetilde{\gamma}(k) = \begin{bmatrix} \gamma(k) & 0 \end{bmatrix}^T \end{cases} \tag{31}$$

The new state quantity $\xi(k)$ contains the control quantity $u(k-1)$ from the previous moment, and the control quantity of the system now becomes the control increment $\Delta u(k)$. In order to be able to make the three-axis heavy vehicle track the transverse swing angle and lateral position of the reference trajectory in the prediction time domain N_p with the first control quantity of the control sequence, the prediction equation of the output quantity in the prediction time domain N_p is constructed as follows:

$$\widetilde{\eta}(k) = \Psi \xi(k) + \Theta \Delta U(k) + \Gamma \Xi(k) \tag{32}$$

$$\widetilde{\eta}(k) = \left[\eta(k+1), \eta(k+2), \cdots, \eta(k+N_c), \cdots, \eta(k+N_p)\right]^T \tag{33}$$

$$\Psi = \left[\widetilde{C}_k \widetilde{A}_k, \widetilde{C}_k \widetilde{A}_k^2, \cdots, \widetilde{C}_k \widetilde{A}_k^{N_c}, \cdots, \widetilde{C}_k \widetilde{A}_k^{N_p}\right]^T \tag{34}$$

$$\Delta U(k) = \left[\Delta u(k), \Delta u(k+1), \cdots, \Delta u(k+N_c-1)\right]^T \tag{35}$$

$$\Xi(k) = \left[\widetilde{\gamma}(k), \widetilde{\gamma}(k+1), \cdots, \widetilde{\gamma}(k+N_c), \cdots, \widetilde{\gamma}(k+N_p-1)\right]^T \tag{36}$$

$$\Theta = \begin{bmatrix} \widetilde{C}_k \widetilde{B}_k & 0 & \cdots & 0 \\ \widetilde{C}_k \widetilde{A}_k \widetilde{B}_k & \widetilde{C}_k \widetilde{B}_k & \cdots & 0 \\ \vdots & \vdots & \ddots & \vdots \\ \widetilde{C}_k \widetilde{A}_k^{N_c-1} \widetilde{B}_k & \widetilde{C}_k \widetilde{A}_k^{N_c-2} \widetilde{B}_k & \cdots & \widetilde{C}_k \widetilde{B}_k \\ \vdots & \vdots & \ddots & \vdots \\ \widetilde{C}_k \widetilde{A}_k^{N_p-1} \widetilde{B}_k & \widetilde{C}_k \widetilde{A}_k^{N_p-2} \widetilde{B}_k & \cdots & \widetilde{C}_k \widetilde{A}_k^{N_p-N_c} \widetilde{B}_k \end{bmatrix} \tag{37}$$

$$\Gamma = \begin{bmatrix} \widetilde{C}_k & 0 & \cdots & 0 \\ \widetilde{C}_k \widetilde{A}_k & \widetilde{C}_k & \cdots & 0 \\ \vdots & \vdots & \ddots & \vdots \\ \widetilde{C}_k \widetilde{A}_k^{N_p-1} & \widetilde{C}_k \widetilde{A}_k^{N_p-2} & \cdots & \widetilde{C}_k \end{bmatrix} \tag{38}$$

The predicted output quantity $Y(k)$ contains all the outputs in the predicted time domain N_p, while the control sequence $\Delta U(k)$ acts only in the control time domain N_c.

With the output prediction equation and the control sequence $\Delta U(k)$ in the prediction time domain N_p, the following objective function is defined as follows:

$$J = \left(\widetilde{\eta} - \widetilde{\eta}_{ref}\right) Q \left(\widetilde{\eta} - \widetilde{\eta}_{ref}\right)^T + \Delta U^T R \Delta U + \rho \varepsilon^2 \tag{39}$$

where Q and R are coefficient matrices that serve to determine the weight of each parameter and control quantity in the output quantity in the optimization solution process.

To ensure that the optimization problem is always solvable, the relaxation variable ε and its corresponding weight coefficient ρ are added. The solution process also requires adding constraints to the increments of the control quantity $\Delta u(k)$, the control quantity $u(k)$, and the output quantity y.

The increments of the control quantities and the constraints on the control quantities are as follows:

$$\Delta u_{\min} \le \Delta u(k) \le \Delta u_{\max} \tag{40}$$

$$u_{\min} \le u(k) \le u_{\max} \tag{41}$$

Equation (39) is reduced to a standard quadratic form in order to facilitate the solution as follows:

$$\begin{aligned} J &= \begin{bmatrix} \Delta U(k)^T & \varepsilon \end{bmatrix} \begin{bmatrix} \Theta^T Q \Theta + R & 0 \\ 0 & \rho \end{bmatrix} \begin{bmatrix} \Delta U(k) \\ \varepsilon \end{bmatrix} + 2 \begin{bmatrix} E & 0 \end{bmatrix} \begin{bmatrix} \Delta U(k) \\ \varepsilon \end{bmatrix} \\ s.t. \quad & \mathrm{K} \begin{bmatrix} \Delta U(k) \\ \varepsilon \end{bmatrix}^T \ll \Omega \end{aligned} \tag{42}$$

$$I_u = \begin{bmatrix} 1 & 0 & \cdots & 0 \\ 0 & 1 & \cdots & 0 \\ \vdots & \vdots & \ddots & \vdots \\ 0 & 0 & \cdots & 1 \end{bmatrix}_{N_c \times N_c} \tag{43}$$

$$E = (\Psi \xi(k))^T Q \Theta + (\Gamma \Xi(k))^T Q \Theta - \widetilde{\eta}_{ref}^T Q \Theta \tag{44}$$

$$L_u = \begin{bmatrix} 1 & 0 & \cdots & 0 \\ 1 & 1 & \cdots & 0 \\ \vdots & \vdots & \ddots & \vdots \\ 1 & 1 & \cdots & 1 \end{bmatrix}_{N_c \times N_c} \tag{45}$$

$$\Omega = \begin{bmatrix} -\Delta U_{\min} \\ \Delta U_{\max} \\ -U_{\min} + U(k-1) \\ U_{\max} - U(k-1) \\ -\widetilde{\eta}_{\min} + \Psi \xi(k) + \Gamma \Xi(k) \\ \widetilde{\eta}_{\max} - \Psi \xi(k) - \Gamma \Xi(k) \end{bmatrix} \tag{46}$$

$$\mathrm{K} = \begin{bmatrix} -I_u & I_u & -L_u & L_u & -\Theta & \Theta \\ 0 & 0 & 0 & 0 & 0 & 0 \end{bmatrix}^T \tag{47}$$

3.3. Longitudinal Motion Controller

Control of the vehicle speed with first-order inertial systems as follows:

$$\dot{a} = \frac{1}{\tau_d}(a_d - a) \tag{48}$$

where τ_d is the time constant, and a_d is the desired acceleration.

$$x(k+1) = Ax(k) + Bu(k) \tag{49}$$

Among them,

$$A_k = \begin{bmatrix} 1 & T \\ 0 & 1 - \frac{T}{\tau_d} \end{bmatrix} \tag{50}$$

$$B_k = \begin{bmatrix} 0 & \frac{T}{\tau_d} \end{bmatrix}^T \tag{51}$$

where $\boldsymbol{x}(k) = [v, a]^T$ is the system state quantity, and $\boldsymbol{u}(k) = a_{\mathrm{r}}(k)$ is the system input quantity.

The velocity $v(k)$ is used as the system output, and the output equation can be expressed as follows:

$$y(k) = Cx(k) \tag{52}$$

The longitudinal motion upper controller is designed based on the model predictive control approach. Similar to the derivation process of the transverse controller, the final velocity control problem is transformed into solving the following optimization problem.

$$\begin{aligned} &\min_{k=1,\ldots,N_p} J = \sum_k \|y(k) - v_r(k)\|_Q^2 + \sum_k \|\Delta u(k)\|_R^2 + \rho\varepsilon^2 \\ &s.t. \qquad \Delta u_{\min} \le \Delta u(k) \le \Delta u_{\max} \\ &\qquad\quad u_{\min} \le u(k) \le u_{\max} \end{aligned} \tag{53}$$

The optimization problem is solved using the quadratic programming library function.

The design of the lower controller based on the reference acceleration is calculated by the upper controller. The feedforward vehicle speed controller is designed to compensate for the longitudinal vehicle speed. The vehicle longitudinal dynamics are modeled as follows:

$$m\dot{v}_x = F_{xf} + F_{xm} + F_{xr} \tag{54}$$

Equation (49) is subtracted from Equation (1) to obtain

$$\Delta F_x = F_{xf} - F_{xf}\cos\delta_f + F_{yf}\sin\delta_f - mv_y(\dot{\varphi} + \dot{\beta}) \tag{55}$$

$$F_t = F_f + F_w + F_i + F_j \tag{56}$$

where F_{t} is the driving force, F_{f} is the rolling resistance, F_{w} is the air resistance, F_{i} is the acceleration resistance, and F_{j} is the acceleration resistance.

The driving force is calculated as follows:

$$F_t = \frac{T_{tq} i_g i_0 \eta_t}{r} \tag{57}$$

where T_{tq} is the engine torque, i_g is the transmission ratio, i_0 is the torque converter ratio, η_t is the transmission system transmission efficiency, and r is the dynamic radius of the truck wheel.

The rolling resistance is calculated by Equation (58) as follows:

$$F_f = mgf \tag{58}$$

where f is the rolling resistance coefficient.

The acceleration resistance is as follows:

$$F_j = ma_r \tag{59}$$

From Equation (49)–Equation (54), it is obtained that

$$ma_r = \frac{T_{tq} i_g i_0 \eta_t}{r} - mgf - \Delta F_x \tag{60}$$

To simplify the control, it is assumed that the magnitude of the throttle opening u_T is linearly related to the reference acceleration as follows:

$$u_T = k_T \left(a_r(k) - \frac{\Delta F_x}{m} \right) \tag{61}$$

When the vehicle is in the stability domain, the value of the state matrix Q is set to Q_1, the coefficient corresponding to the lateral eccentricity of the center of mass is 0, and the braking torque is distributed equally, when the lateral motion controller mainly ensures the tracking performance. The braking torque of each wheel is as follows:

$$F_{b,xi} = k_{b,T} a_r(k) \tag{62}$$

When the vehicle is in the instability interval, the state matrix Q is set as Q_2, and the influence of the lateral deflection angle of the center of mass on the vehicle stability is considered in the tracking process. Multiple wheels are coordinated and controlled according to the attachment of each wheel of the three-axle heavy vehicle, and longitudinal braking moments are generated at each wheel by means of the optimal braking force distribution, and the difference between the longitudinal braking moments on the left and right wheels constitutes the additional transverse moment.

The objective function of the braking force distribution is as follows:

$$\min J = \sum_{i=1}^{6} \frac{F_{b,xi}^2}{(\mu F_{zi})^2} \tag{63}$$

where $F_{b,xi}$ is the braking force applied to each tire.

The constraints on the braking force distribution include an equation constraint and an inequality constraint. The equation constraint is that the sum moment produced by the braking force applied on each wheel of the three-axle heavy vehicle to the center of mass of the vehicle is the additional transverse sway moment. At the same time, the generated braking force has to satisfy the tire friction circle constraint. In summary, the braking force distribution constraint is as follows:

$$-\frac{l_w}{2}(F_{b,x1} - F_{b,x2} + F_{b,x3} - F_{b,x4} + F_{b,x5} - F_{b,x6}) = M \tag{64}$$

$$-\sqrt{\mu^2 F_{zi}^2 - F_{yi}^2} \leq F_{b,xi} \leq 0 \tag{65}$$

The formula for calculating the braking torque on each tire is as follows:

$$T_{bi} = F_{b,xi} R_t \tag{66}$$

where R_t is the wheel radius.

3.4. Speed Planning

In order to improve the rollover stability of three-axle heavy vehicles during tracking control, a real-time speed planning method considering the rollover stability of three-axle heavy vehicles is proposed.

In a conventional vehicle, the driver will accelerate or decelerate in advance according to the current vehicle state and the road condition ahead to prevent the vehicle from overturning. Similar to the driver's operation, this paper uses a two-point pre-sighting to limit the maximum vehicle speed V_{max}, as shown in Figure 4. P_1 indicates the current center-of-mass position of the vehicle, and P_2 is the pre-sighting point that changes with the current vehicle speed.

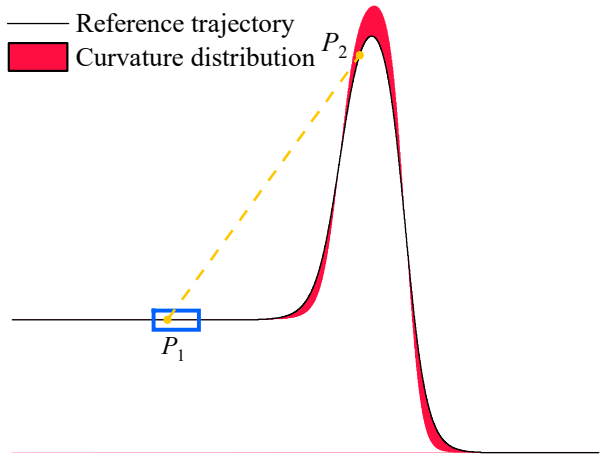


Figure 4. Diagram of vehicle speed pre-sighting.

First, the lateral load transfer rate at the current position P_1 of the vehicle is calculated.

$$LTR = \frac{|F_{zr} - F_{zl}|}{F_{zr} + F_{zl}} = \frac{K_\phi \sin\phi + C_\phi \dot{\phi} \cos\phi}{mgl_w} \tag{67}$$

Next, the pre-sighting distance $d_p(k)$ is calculated based on the current vehicle speed, and the calculation formula can be expressed as follows:

$$d_p(k) = d_r(k) + \lambda v_r(k) \tag{68}$$

where λ is the pre-scanning distance weighting factor.

Then, the road curvature κ at the pre-sighting point P_2 is calculated based on the pre-sighting distance $d_p(k)$. All the systems involved in this paper are discretized in order to facilitate processing by digital computers. In addition, most path planning methods plan the reference path as road coordinates without analytical expressions. Therefore, the road curvature needs to be calculated based on the discretized coordinate points. Assuming that the horizontal and vertical coordinates of the reference path are (x, y), the coordinates of the reference curvature in the continuous system are as follows:

$$\kappa = \frac{|x''y' - x'y''|}{\left((x')^2 + (y')^2\right)^{\frac{3}{2}}} \tag{69}$$

The formula for calculating the maximum vehicle speed is

$$V_{max} = V_{max0} - \max(\mu_1 LTR, \mu_2 \kappa) \tag{70}$$

where V_{max0} is the initial maximum speed, and μ_1 and μ_2 are the speed limit weighting factors.

With a limit on the maximum vehicle speed based on rollover stability, the next step is to design a speed planning strategy.

The driving process of the dump truck from the starting point to the end point goes through the stages of acceleration, uniformity, and deceleration. Assuming that the distance d_0, velocity v_0, and acceleration a_0 traveled by the vehicle at the starting point are zero, the following velocity planning model is established as follows:

$$a_{\mathrm{r}} = \int j dt = a_0 + jt \tag{71}$$

$$v_{\mathrm{r}} = \int a dt = v_0 + a_0 t + \frac{1}{2} j t^2 \tag{72}$$

$$d_{\mathrm{r}} = \int v dt = S_0 + v_0 t + \frac{1}{2} a_0 t^2 + \frac{1}{6} j t^3 \tag{73}$$

where j is the reference acceleration change rate, $\mathrm{a_r}$ is the reference acceleration, $\mathrm{v_r}$ is the reference speed, and d_r is the reference travel distance. In order to adjust the planned reference speed according to the actual operating state of the vehicle during the vehicle driving process, the currently planned reference acceleration $a_r(k)$, reference speed $v_r(k)$, and reference travel distance $d_r(k)$ are taken as the state quantity $S(k)$; the travel acceleration change rate $j(k)$ is taken as the control quantity; and the system sampling time is ΔT, which can be obtained as a speed planning state equation from Equations (71)–(73).

$$S(k+1) = A_s S(k) + B_s j(k) \tag{74}$$

$$S(k) = \begin{bmatrix} a_r(k) & v_r(k) & d_r(k) \end{bmatrix}^T \tag{75}$$

$$B_s = \begin{bmatrix} \Delta T & \frac{\Delta T^2}{2} & \frac{\Delta T^3}{6} \end{bmatrix}^T \tag{76}$$

$$A_s = \begin{bmatrix} 1 & 0 & 0 \\ \Delta T & 1 & 0 \\ \frac{\Delta T^2}{2} & \Delta T & 1 \end{bmatrix} \tag{77}$$

In lateral motion control, the reference lateral displacement of the vehicle in the predicted time domain N_{p} and the corresponding reference transverse sway angle need to be provided. Therefore, model predictive control is used to plan the velocity, acceleration, and distance in the predicted time domain N_{p}. The prediction equations are as follows:

$$S(k+1) = \widetilde{A}_s S(k) + \widetilde{B}_s j(k) \tag{78}$$

$$\widetilde{A}_s = \begin{bmatrix} A_s & A_s^2 & \cdots & A_s^{N_p} \end{bmatrix}^T \tag{79}$$

$$\widetilde{B}_s = \begin{bmatrix} B_s & 0 & \cdots & 0 \\ A_s B_s & B_s & \cdots & 0 \\ \vdots & \vdots & \ddots & \vdots \\ A_s^{N_p-1} B_s & A_s^{N_p-2} B_s & \cdots & B_s \end{bmatrix} \tag{80}$$

The process of vehicle driving from the starting point to the end point can be generally divided into three stages: acceleration, uniform speed, and deceleration. The acceleration and deceleration switching strategy is designed by combining the reference velocity v_r and reference acceleration a_r of the current moment planned by the vehicle, as shown in Figure 5.

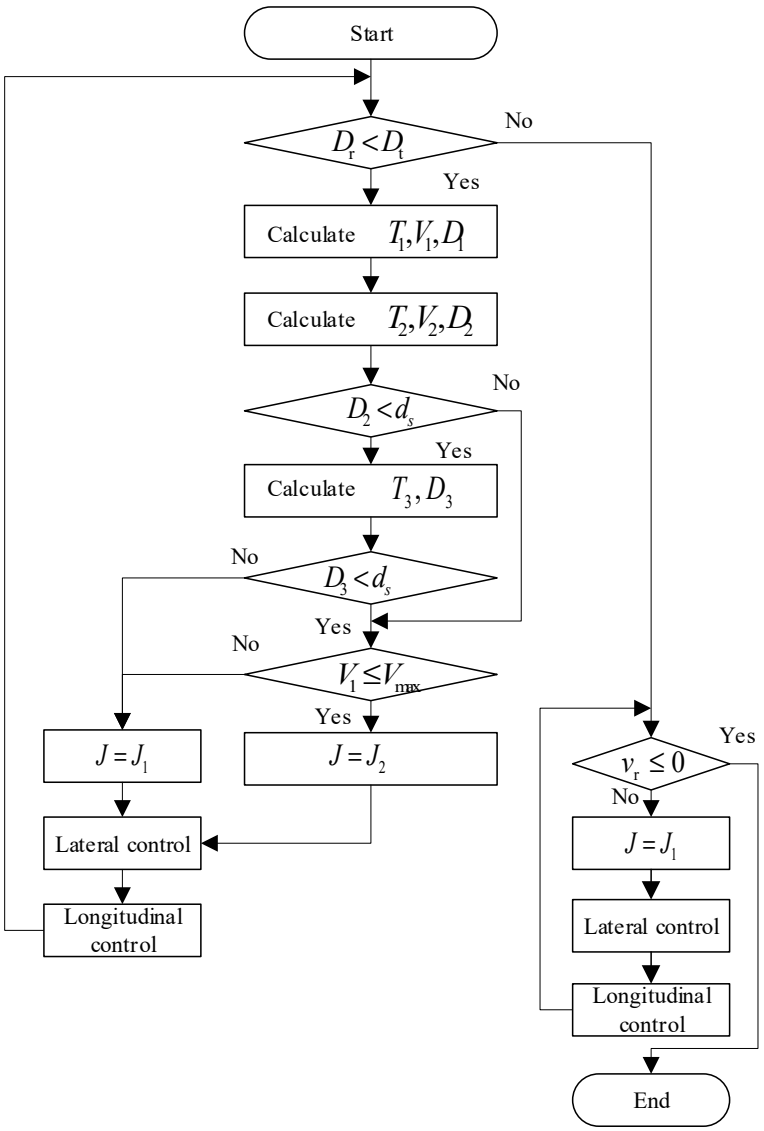


Figure 5. Flow chart of the speed planning strategy.

When the vehicle does not reach the end point ($D_r < D_t$), if the current reference acceleration is planned $a_r > 0$, that the vehicle is in the acceleration phase. It needs to calculate the time T_1, the velocity V_1 after the time T_1, and the total distance travelled D_1 firstly, which are required to reduce the current acceleration a_r to 0.

If the vehicle reaches the end point before the acceleration reaches the minimum value, the objective function J_1 is set to minimize the vehicle acceleration.

If the reference acceleration decreases to a minimum value, i.e., the vehicle still does not reach the end of the line when the maximum deceleration is reached, then the vehicle will travel in a uniform deceleration motion. If the vehicle reaches the end of the line during the deceleration to 0, the objective function is set to J_1.

If the speed decreases to 0 when the vehicle still has not reached the end, then the vehicle needs to continue to accelerate forward, and to ensure that the maximum speed does not exceed the set upper limit $V_{\max}$, because the acceleration is reduced to 0 when the speed is maximum, the speed is V_1, so when $V_1 > V_{\max}$, set the objective function for J_1, so that the vehicle decelerates; when $V_1 < V_{\max}$, set the objective function for J_2, so that the vehicle accelerates. The final speed will fluctuate around the $V_{\max}$.

If the reference acceleration of the vehicle at the current moment is less than 0, it means that the vehicle is about to reach the end point at this moment or is in the deceleration state

in order to meet the vehicle dynamics constraints and still needs to plan the speed and acceleration of the future moment according to the planned distance between the vehicle and the end point.

Similar to the reference acceleration greater than 0, if the vehicle has reached the end point when the acceleration reaches the minimum value or the vehicle travel speed decreases to 0, then decelerate the vehicle; otherwise, accelerate the vehicle without exceeding the maximum speed. Calculate *Ti*, *Vi*, *Di*, and J_{ii} in different cases, respectively, where $i = 1, 2, 3$; $ii = 1, 2$. The calculation formula is as follows:

$$T_1 = \left| \frac{a_r}{j_{\min}} \right| \tag{81}$$

$$V_1 = \begin{cases} v_r + a_r T_1 + \frac{1}{2} J_{\min} T_1^2 & a_r \geq 0 \\ v_r + a_r T_1 + \frac{1}{2} J_{\max} T_1^2 & a_r < 0 \end{cases} \tag{82}$$

$$D_1 = d_r + v_r T_1 + \frac{1}{2} a_r T_1^2 + \frac{1}{6} j_{\min} T_1^3 \tag{83}$$

$$T_2 = \left| \frac{a_{\min}}{j_{\min}} \right| \tag{84}$$

$$V_2 = \begin{cases} V_1 + \frac{1}{2} J_{\min} T_2^2 & a_r \geq 0 \\ v_r + a_r T_2 + \frac{1}{2} J_{\min} T_2^2 & a_r < 0 \end{cases} \tag{85}$$

$$D_2 = \begin{cases} D_1 + V_1 T_2 + \frac{1}{6} j_{\min} T_2^3 & a_r \geq 0 \\ d_r + v_r T_2 + \frac{1}{2} a_r T_2^2 + \frac{1}{6} j_{\min} T_2^3 & a_r < 0 \end{cases} \tag{86}$$

$$T_3 = \left| \frac{V_2}{a_{\min}} \right| \tag{87}$$

$$D_3 = D_2 + V_2 T_3 + \frac{1}{2} a_{\min} T_3^2 \tag{88}$$

Therefore, the speed planning problem is transformed into solving the following optimization problem:

$$\begin{aligned} &\min_{k=0,1,\ldots,N_p} J = J_1 \text{ or } J_2 \\ &s.t. \quad S_{\min} \leq S(k) \leq S_{\min} \end{aligned} \tag{89}$$

Among them,

$$J_1 = \sum_{i=1}^{N_p} C_a S(k+i) \tag{90}$$

$$J_2 = -J_1 \tag{91}$$

$$C_a = \begin{bmatrix} 1 & 0 & 0 \end{bmatrix}^T \tag{92}$$

The optimization problem can be solved in Matlab by calling the function fmincon [32] or linprog [33].

4. Simulation Analysis

Trucksim and Simulink are used to simulate a three-axle heavy-duty vehicle under the uniform speed condition and the transverse–longitudinal coordinated control condition to verify the capability of the proposed horizontal and vertical coordinated control strategy in terms of tracking control, stability control, and speed planning. The input of Trucksim is the front wheel rotation angle, throttle opening, and braking torque of each wheel; the output of Trucksim is the transverse–longitudinal speed, transverse-swing angular velocity,

lateral camber angular velocity, and transverse–longitudinal coordinates of the vehicle in the inertial coordinate system.

The parameters are calibrated based on the parameters of an actual specific three-axis vehicle. The main parameters of the selected three-axle heavy vehicle are shown in Table 2.

Table 2. The main parameters of the vehicle table.

Parameter	Symbol	Unit	Value
Spring mass	m	mg	6310
Dynamic radius of the truck wheel	r	m	0.55
Distance from centroid to front axle	l_f	m	1.385
Distance from centroid to middle axle	l_m	m	3.115
Distance from centroid to rear axle	l_r	m	4.385
Roll arm length	h	m	0.629
Vehicle width	l_w	m	1.95
The moment of inertia around the x-axis	I_x	kg·m^2	6879
The moment of inertia around the z-axis	I_z	kg·m^2	19,665
Equivalent roll stiffness of suspension	K_φ	N·m/rad	378,152
Equivalent roll damping of suspension	C_φ	N·m·s/rad	18,908

In the uniform speed condition, the speed is set to 18 m/s, and the reference acceleration and reference acceleration change rate are 0. In the transverse–longitudinal coordination control condition, the vehicle is set to start from the starting point, and the initial speed, acceleration, and acceleration change rate are 0, and the initial maximum speed is 18 m/s. Set the limit lane change trajectory scene: At a certain moment during the uniform speed of the vehicle, the limit lane change is carried out—first to the left, then to the right, and finally to the right lane of the initial lane. The simulation results are shown in Figure 6.

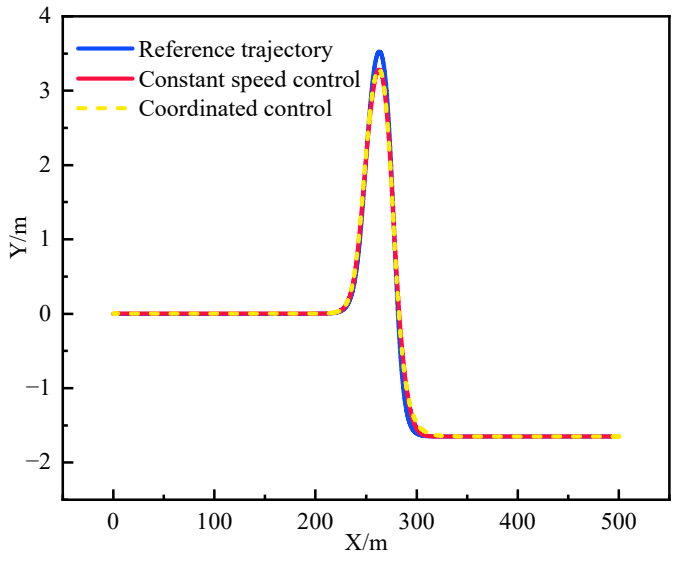


Figure 6. Simulation results of the horizontal and vertical coordinated control.

From Figure 6, it can be seen that the horizontal and vertical coordinated control strategy designed in this section under the speed change condition can track the reference trajectory well.

It can be seen from Figures 7 and 8 that the reference speed and reference acceleration both increase gradually from 0 after the simulation starts. When the time is 1.9 s, the reference acceleration reaches the upper limit value of 1 m/s^2, and the reference vehicle

speed enters the phase of linear increase. When the time is 21.2 s, the reference speed reaches the maximum value of 18 m/s. When the time is 14.9 s, the maximum speed starts to decrease, because the curvature at the pre-targeting point P_2 starts to increase significantly. Then, the curvature at the pre-sighting point P_2 gradually returned to normal, the upper speed limit rebounded briefly, and the vehicle reached the maximum value of 18 m/s at 21.2 s. Then, the vehicle entered the large curvature section, the lateral load transfer rate at point P_1 began to rise, and the upper speed limit fluctuated. When the time is 29.1 s, the vehicle drives through the large curvature section, the transverse load transfer rate at the P1 point gradually decreases, the upper speed limit gradually rises back to 18 m/s, and the reference speed continues to rise. By 33.6 s, the reference speed reaches 14.6 m/s and starts to decelerate according to the speed planning strategy, and the reference acceleration gradually decreases to the minimum value. When the time is 49.2 s, the reference speed is close to 0 m/s so that the vehicle reaches the terminal, and the simulation ends with the reference acceleration set to zero.

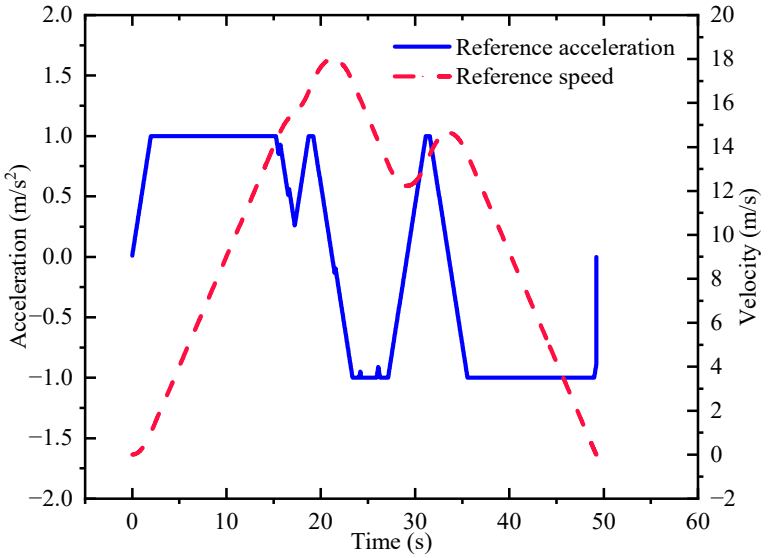


Figure 7. Acceleration simulation results.

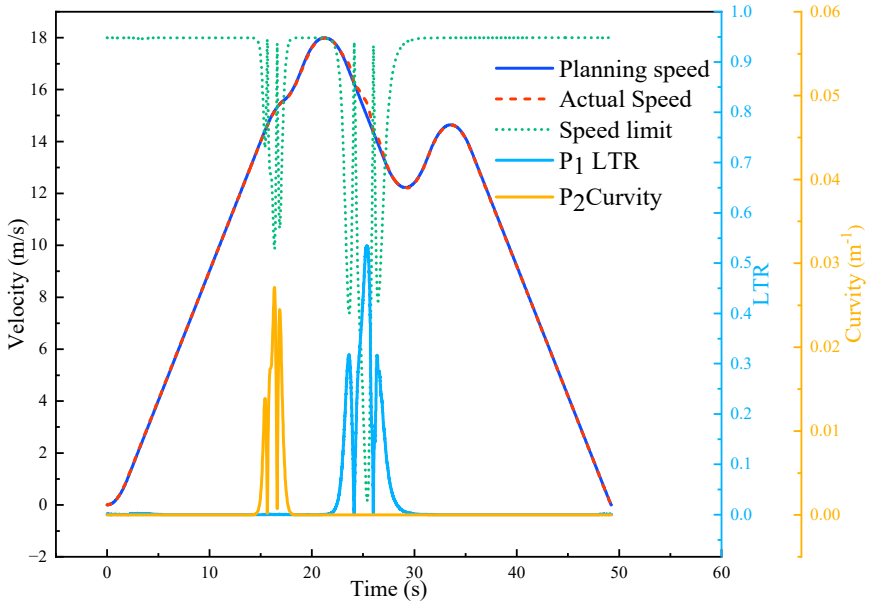


Figure 8. Speed simulation results.

It can be seen from Figure 9 that the absolute value of the speed tracking error is 0.35 m/s, the absolute value of the lateral position tracking error is 0.37 m, and the absolute value of the heading angle tracking error is 0.07 rad at the constant speed control. From Figure 10, it can be seen that, under the horizontal and vertical coordinated control strategy, the maximum speed tracking error is 0.5 m/s, the maximum horizontal position tracking error is 0.6 m, and the maximum heading angle tracking error is 0.12 rad. Both the lateral motion control and the transverse–longitudinal coordinated control algorithm can track the reference trajectory well under the uniform speed condition.

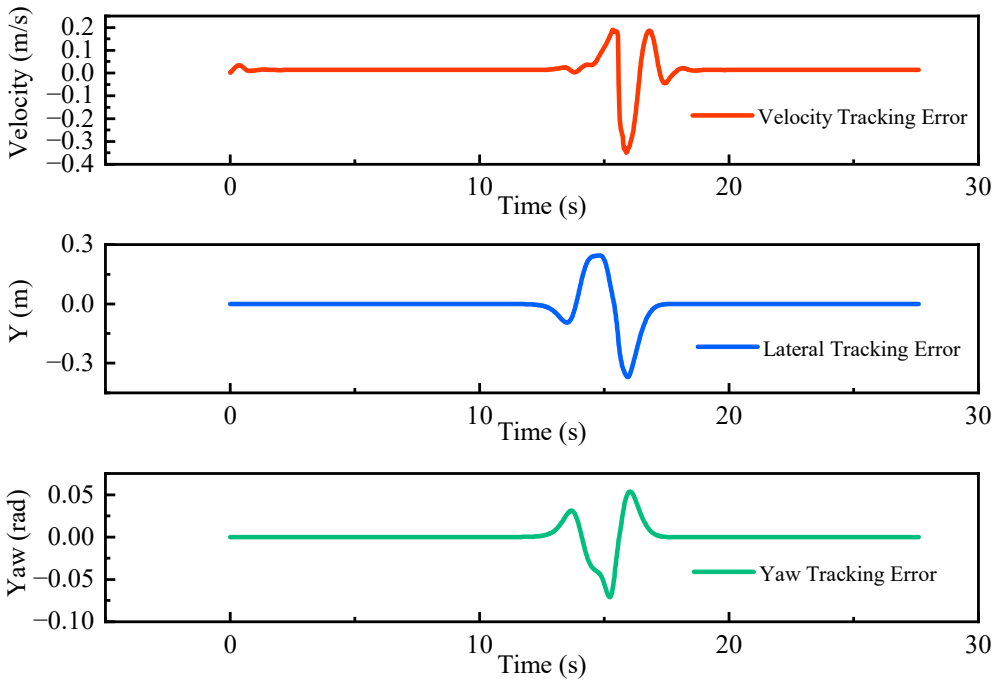


Figure 9. Tracking error under the constant speed control.

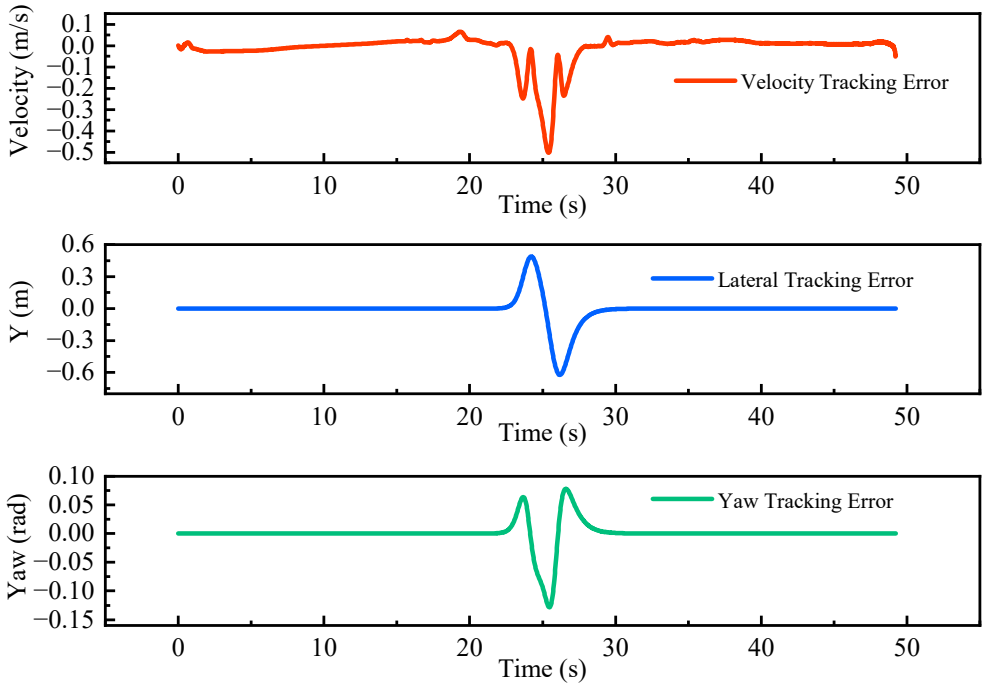


Figure 10. Horizontal and vertical coordination control tracking errors.

Figure 11, Figure 12, and Table 3 show the transverse angular velocity and lateral acceleration of the vehicle under the two algorithms, respectively. The peak absolute values of transverse angular velocity and lateral acceleration are 0.39 rad/s and 6.7 m/s^2, respectively, at the constant speed control. Compared to the uniform lateral motion control, the peak values of the transverse angular velocity and peak absolute values of lateral acceleration of the vehicle are 0.34 rad/s and 5.2 m/s^2, respectively, when using the horizontal and vertical coordinated control strategy, which are reduced by 14.1% and 22.4%, respectively.

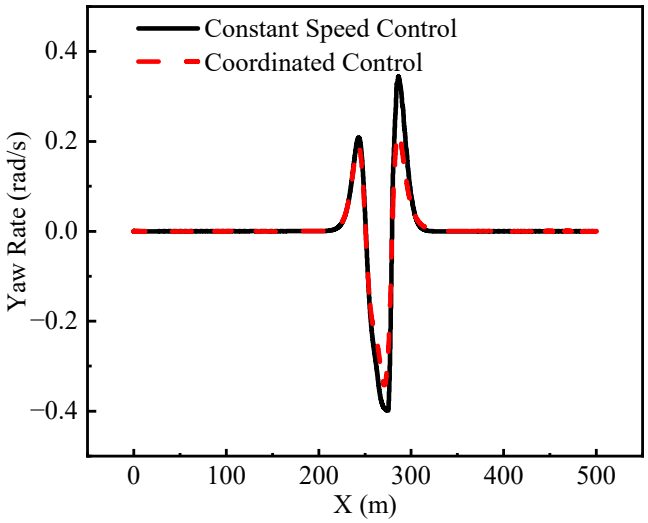


Figure 11. Comparison of the yaw rate.

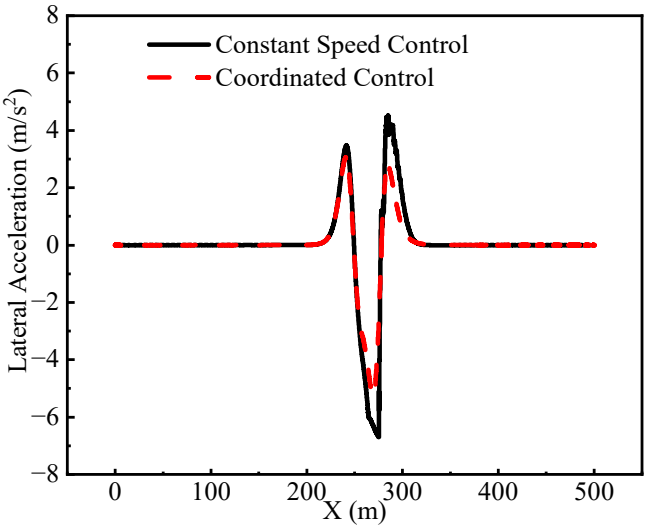


Figure 12. Comparison of the lateral acceleration.

Table 3. The peak values of the yaw rate and lateral acceleration.

	Constant Speed Control	Coordination Control	Optimization
Yaw rate (rad/s)	0.39	0.34	14.1%
Lateral acceleration (m/s^2)	6.7	5.2	22.4%

As can be seen from Figure 13 and Table 4, when the three-axle heavy vehicle is driving at a uniform speed of 18 m/s, the maximum value of the transverse load transfer rate can reach 0.73. Under the transverse–longitudinal coordination control strategy, the maximum transverse load transfer rate is 0.53, which decreases by 20% and effectively avoids the occurrence of rollover.

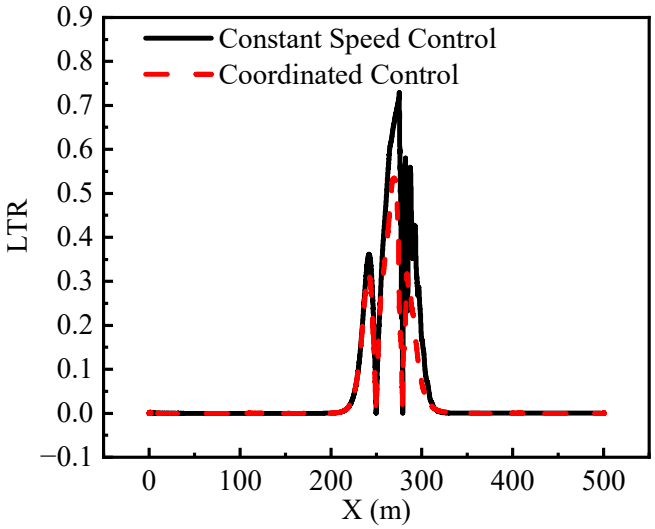


Figure 13. Comparison of the lateral transfer rate.

Table 4. The peak value of the lateral transfer rate.

	Constant Speed Control	Coordination Control	Optimization
lateral transfer rate	0.73	0.53	20%

From Figures 14 and 15 and Table 5, it can be seen that the peak absolute value of the mass side deflection angle can reach 0.05 rad under the uniform speed condition, while the peak absolute value of the mass side deflection angle is 0.02 rad using the horizontal and vertical coordinated control strategy.

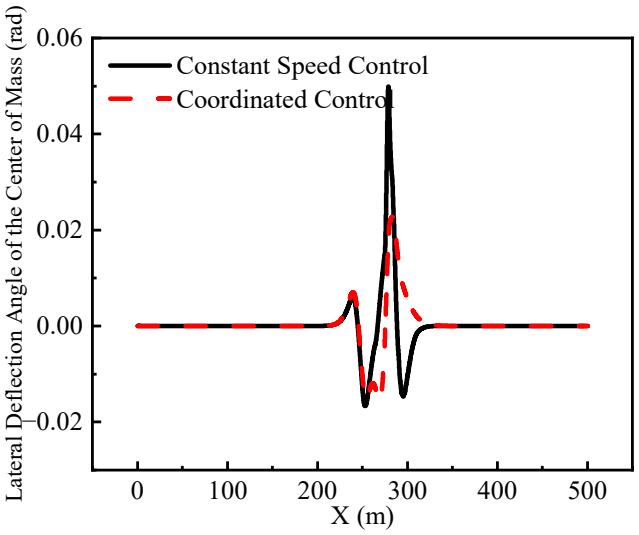


Figure 14. Comparison of the lateral deflection angle of the center of mass.

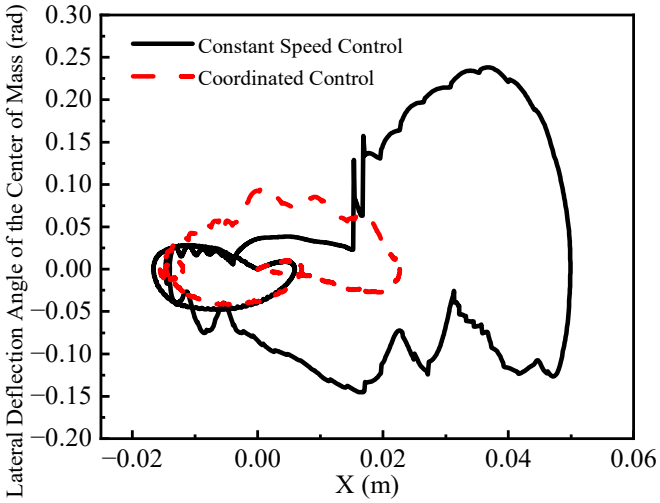


Figure 15. Phase trajectory comparison.

Table 5. The peak value of the lateral deflection angle of the center of mass.

	Constant Speed Control	Coordination Control	Optimization
lateral deflection angle of the center of mass (rad)	0.05	0.02	60%

As can be seen from Figure 16, when the distance between the starting point and the end point is 500 m, the vehicle is still a certain distance from the end point after driving through the large curvature section and starts to increase its speed from 29.1 s. While when the distance between the starting point and the end point is 120 m and 300 m, the vehicle speed starts to slow down from 12.0 s and 18.5 s, respectively, because the distance is shorter, and the speed has not reached the maximum. Eventually, the vehicle that arrived at the end had the speed reduced to 0 m/s.

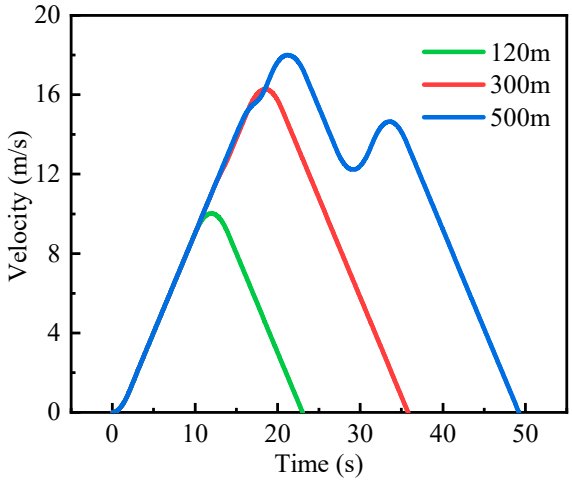


Figure 16. Planned speed curves under different path lengths.

5. Summary

In this paper, a three-axis heavy-duty vehicle is taken as the research object, and the horizontal and vertical coordinated control strategy of the vehicle under variable-speed working conditions is designed. A tire model is constructed based on the magic formula for analyzing the transverse and longitudinal mechanical properties of the vehicle in motion.

The transverse motion controller is designed based on the phase plane method so that it can ensure the transverse sway stability of the vehicle while tracking the reference path. The braking moment of each wheel is redistributed by the quadratic planning method, and the sum moment produced by the braking force on the vehicle center of mass is the additional transverse sway force dipole moment.

Based on this, a velocity planning method is designed, which plans a velocity pro-file from the starting point to the end point based on the lateral load transfer rate of the three-axle heavy vehicle at the current moment and the road curvature at the pre-sighting point and makes the three-axle heavy vehicle meet the requirements of lateral stability and the acceleration and velocity limits. The speed of the vehicle at the starting point and at the end point is 0.

The simulation results show that the coordinated transverse–longitudinal control strategy under variable speed conditions can ensure the transverse sway stability and lateral sway stability of the three-axle heavy-duty vehicle while accurately tracking the reference trajectory. Compared to the uniform speed condition, the peak transverse angular velocity and peak lateral acceleration of the vehicle decreased by 14.1% and 22.4%, respectively, and the lateral load transfer rate decreased by 20%. This indicates an improvement in both the vehicle's sway stability and rollover protection. As the closed-loop system has no stability guarantees, this control mentioned is a proposal limitation.

To achieve precise trajectory tracking in dynamic environments while ensuring lateral stability and roll stability, a vehicle horizontal and vertical coordinated control strategy based on model predictive control (MPC) typically requires the integration of multiple sensor inputs and processing of environmental factors. Future research will consider the combination of the vehicle stability, optimizing the coupling relationship between vehicle speed control and steering angle, to reduce the risk of vehicle sideslip or instability.

Author Contributions: Conceptualization, L.Z.; Methodology, L.Z.; Formal analysis, H.C.; Investigation, L.Z. and Y.W.; Writing—original draft, F.H.; Writing—review & editing, L.Z.; Visualization, L.Z. and L.Y.; Supervision, L.Y. All authors have read and agreed to the published version of the manuscript.

Funding: This research was funded by the Natural Science Research Project of Higher Education Institutions in Jiangsu Province (grant number 22KJD440001, 22KJA580002, 24KJA580003) and Changzhou Science & Technology Program (grant number CJ20220232).

Data Availability Statement: The original contributions presented in this study are included in the article. Further inquiries can be directed to the corresponding author.

Conflicts of Interest: The authors declare no conflicts of interest.

References

1. Wang, H.; Hou, L.; Shangguan, W.-B. Research on vehicle rollover warning and braking control system based on secondary predictive zero-moment point position. *SAE Int. J. Adv. Curr. Pract. Mobil.* **2022**, *4*, 1689–1703. [CrossRef]
2. Wu, X.; Li, T. A deep learning-based car accident detection approach in video-based traffic surveillance. *J. Opt.* **2024**, *53*, 3383–3391. [CrossRef]
3. Sukumaran, R.; Gaurkar, P.V.; Subramanian, S.C. Integrated Rollover Prevention and Antilock Brake System for Heavy Commercial Road Vehicles. *IEEE Access* **2023**, *11*, 124081–124097. [CrossRef]
4. Wang, M.; Liu, J.; Zhang, H.; Gan, L.; Xu, X.; He, J.; Chen, S. Vehicle rollover warning system based on TTR method with inertial measurement. *Meas. Sci. Technol.* **2021**, *33*, 015108. [CrossRef]
5. Chen, Y.H.; Xu, J.K.; Mao, J.G.; Jin, Z.L. Research on Vehicle Rollover Warning System. *Appl. Mech. Mater.* **2014**, *590*, 437–441. [CrossRef]
6. Chao, P.P.; Zhang, R.Y.; Wang, Y.D.; Tang, H.; Dai, H.L. Warning model of new energy vehicle under improving time-to-rollover with neural network. *Meas. Control J. Inst. Meas. Control* **2022**, *55*, 1004–1015. [CrossRef]

7. Hou, J.; Lei, H.; Fu, Z.; Yuan, P.; Yin, Y.; Feng, H.; Li, Z.; Zhang, M.; Cui, M.; Xu, Y. A Novel Rollover Warning Approach for Commercial Vehicles Using Unscented Kalman Filter. *Math. Probl. Eng.* **2022**, *2022*, 1–13. [CrossRef]
8. Yang, X.; Wu, C.; He, Y.; Lu, X.-Y.; Chen, T. A dynamic rollover prediction index of heavy-duty vehicles with a real-time parameter estimation algorithm using NLMS method. *IEEE Trans. Veh. Technol.* **2022**, *71*, 2734–2748. [CrossRef]
9. Wang, R.; Xu, X.; Chen, S.; Guo, N.; Yu, Z. Vehicle Rollover Warning and Control Based on Attitude Detection and Fuzzy PID. *Appl. Sci.* **2023**, *13*, 4339. [CrossRef]
10. Swethamarai, P.; Lakshmi, P. Adaptive-fuzzy fractional order PID controller-based active suspension for vibration control. *IETE J. Res.* **2022**, *68*, 3487–3502. [CrossRef]
11. Mahmoodabadi, M.; Nejadkourki, N. Optimal fuzzy adaptive robust PID control for an active suspension system. *Aust. J. Mech. Eng.* **2022**, *20*, 681–691. [CrossRef]
12. Li, H.; Zhao, Y.; Lin, F.; Zhu, M. Nonlinear dynamics modeling and rollover control of an off-road vehicle with mechanical elastic wheel. *J. Braz. Soc. Mech. Sci. Eng.* **2018**, *40*, 51. [CrossRef]
13. Liang, J.; Lu, Y.; Pi, D.; Yin, G.; Zhuang, W.; Wang, F.; Feng, J.; Zhou, C. A decentralized cooperative control framework for active steering and active suspension: Multi-agent approach. *IEEE Trans. Transp. Electrif.* **2021**, *8*, 1414–1429. [CrossRef]
14. Ahmadian, N.; Khosravi, A.; Sarhadi, P. Integrated model reference adaptive control to coordinate active front steering and direct yaw moment control. *ISA Trans.* **2020**, *106*, 85–96. [CrossRef]
15. Peng, H.; Wang, W.; An, Q.; Xiang, C.; Li, L. Path tracking and direct yaw moment coordinated control based on robust MPC with the finite time horizon for autonomous independent-drive vehicles. *IEEE Trans. Veh. Technol.* **2020**, *69*, 6053–6066. [CrossRef]
16. Qian, X.; Wang, C.; Zhao, W. Rollover prevention and path following control of integrated steering and braking systems. *Proc. Inst. Mech. Eng. Part D J. Automob. Eng.* **2020**, *234*, 1644–1659. [CrossRef]
17. Fan, B.; Zhang, Y.; Chen, Y.; Meng, L. Intelligent vehicle lateral control based on radial basis function neural network sliding mode controller. *CAAI Trans. Intell. Technol.* **2022**, *7*, 455–468. [CrossRef]
18. Zhao, F.; An, J.; Chen, Q.; Li, Y. Integrated Path Following and Lateral Stability Control of Distributed Drive Autonomous Unmanned Vehicle. *World Electr. Veh. J.* **2024**, *15*, 122. [CrossRef]
19. Parkash, A.; Swarup, A. Application of asymmetric barrier Lyapunov function using ADRC approach for development of autonomous vehicle lateral control. *J. Vib. Control* **2023**, *29*, 2160–2171. [CrossRef]
20. Qin, Z.; Chen, L.; Hu, M.; Chen, X. A lateral and longitudinal dynamics control framework of autonomous vehicles based on multi-parameter joint estimation. *IEEE Trans. Veh. Technol.* **2022**, *71*, 5837–5852. [CrossRef]
21. Junior, A.D.S.; Birkner, C.; Jazar, R.N.; Marzbani, H. Coupled Lateral and Longitudinal Controller for Over-Actuated Vehicle in Evasive Maneuvering with Sliding Mode Control Strategy. *IEEE Access* **2023**, *11*, 33792–33811. [CrossRef]
22. Zhang, L.; Jiang, L.; Liu, H.; Hu, Y.; Wang, P.; Chen, H. Coordinated longitudinal and lateral stability improvement for electric vehicles based on a real-time NMPC strategy. *IEEE Trans. Intell. Transp. Syst.* **2023**, *24*, 5337–5350. [CrossRef]
23. Deepankumar, S.; Jegadheesan, C.; Sathiskumar, S.; Boopalan, N.; Praveenkumar, N.; Arulkumar, S. Design and Fabrication of Vehicle Rollover Prevention by Counter Steering Mechanism. In *Recent Trends in Product Design and Intelligent Manufacturing Systems: Select Proceedings of IPDIMS 2021*; Springer: Berlin/Heidelberg, Germany, 2022; pp. 269–279.
24. Nguyen, T.A. Determination of the rollover limitation of a vehicle when moving by 4-dimensional plots. *Adv. Syst. Sci. Appl.* **2022**, *22*, 96–105.
25. He, Z.; Song, Z.; Wang, L.; Zhou, X.; Gao, J.; Wang, K.; Yang, M.; Li, Z. Fasting the stabilization response for prevention of tractor rollover using active steering: Controller parameter optimization and real-vehicle dynamic tests. *Comput. Electron. Agric.* **2023**, *204*, 107525. [CrossRef]
26. Nguyen, D.N.; Nguyen, T.A.; Dang, N.D. A complex rollover dynamics model with active stabilizer bar controlled by the fuzzy algorithm. *Heliyon* **2022**, *8*, e11715. [CrossRef]
27. González, D.; Milanés, V.; Pérez, J.; Nashashibi, F. In Speed profile generation based on quintic Bézier curves for enhanced passenger comfort. In Proceedings of the 2016 IEEE 19th International Conference on Intelligent Transportation Systems (ITSC), Rio de Janeiro, Brazil, 1–4 November 2016; pp. 814–819.
28. Luo, Y.; Li, S.; Zhang, S.; Qin, Z.; Li, K. Green light optimal speed advisory for hybrid electric vehicles. *Mech. Syst. Signal Process.* **2017**, *87*, 30–44. [CrossRef]
29. Easa, S.M.; Diachuk, M. Optimal speed plan for the overtaking of autonomous vehicles on two-lane highways. *Infrastructures* **2020**, *5*, 44. [CrossRef]
30. Zhang, S.; Wu, S.; Li, D. In A Speed Planning Method Based on Time Domain of Unmanned Ground Vehicle. In Proceedings of the 2021 5th International Conference on Innovation in Artificial Intelligence, Xiamen, China, 5–8 March 2021; pp. 228–233.
31. Bakker, E. A new tire model with an applicationin vehicle dynamics studies. *SAE Tech. Pap.* **1989**, *98*, 890087.

32. Waltz, R.A.; Morales, J.L.; Nocedal, J.; Orban, D. An interior algorithm for nonlinear optimization that combines line search and trust region steps. *Math. Program.* **2006**, *107*, 391–408. [CrossRef]
33. Koberstein, A. Progress in the dual simplex algorithm for solving large scale LP problems: Techniques for a fast and stable implementation. *Comput. Optim. Appl.* **2008**, *41*, 185–204. [CrossRef]

Disclaimer/Publisher's Note: The statements, opinions and data contained in all publications are solely those of the individual author(s) and contributor(s) and not of MDPI and/or the editor(s). MDPI and/or the editor(s) disclaim responsibility for any injury to people or property resulting from any ideas, methods, instructions or products referred to in the content.